# Comparison of multimicrophone probe design and processing methods in measuring acoustic intensity

Curtis P. Wiederhold[a)]
*Department of Mechanical Engineering, Brigham Young University, Provo, Utah 84602*

Kent L. Gee
*Department of Physics and Astronomy, Brigham Young University, Provo, Utah 84602*

Jonathan D. Blotter
*Department of Mechanical Engineering, Brigham Young University, Provo, Utah 84602*

Scott D. Sommerfeldt and Jarom H. Giraud
*Department of Physics and Astronomy, Brigham Young University, Provo, Utah 84602*

(Received 8 October 2013; revised 25 March 2014; accepted 27 March 2014)

Three multimicrophone probe arrangements used to measure acoustic intensity are the four-microphone regular tetrahedral, the four-microphone orthogonal, and the six-microphone designs. Finite-sum and finite-difference processing methods can be used with such probes to estimate pressure and particle velocity, respectively. A numerical analysis is performed to investigate the bias inherent in each combination of probe design and processing method. Probes consisting of matched point sensor microphones both embedded and not embedded on the surface of a rigid sphere are considered. Results are given for plane wave fields in terms of root-mean-square average bias and maximum bias as a function of angle of incidence. An experimental verification of the analysis model is described. Of the combinations considered and under the stated conditions, the orthogonal probe using the origin microphone for the pressure estimate is shown to have the lowest amount of intensity magnitude bias. Lowest intensity direction bias comes from the six-microphone probe using an average of the 15 intensity components calculated using all microphone pairs. Also discussed are how multimicrophone probes can advantageously use correction factors calculated from a numerical analysis and how the results of such an analysis depend on the chosen definition of the dimensionless frequency.
 [http://dx.doi.org/10.1121/1.4871180]

PACS number(s): 43.58.Fm, 43.20.Fn [DKW] Pages: 2797–2807

## I. INTRODUCTION

In the late 1970s a method was developed to estimate active intensity in one dimension by taking the cross-spectral density of two closely-spaced microphone signals.[1–3] This process, called the *p-p* technique,[4] estimates the pressure at the point midway between the two microphones as the mean of the two and estimates the particle velocity at the same point using a finite-difference approximation of the pressure gradient. With pressure and particle velocity estimated, active intensity can be calculated, making the *p-p* technique useful in characterizing sound fields. Study of acoustic intensity has also focused on the use of probes that measure the particle velocity directly, called the *p-u* technique.[5,6] Techniques to use spherical beamforming to measure intensity using multimicrophone probes have also been developed.[7,8]

In the *p-p* probe case, a two-microphone probe measures the component of the acoustic intensity along the line from one transducer's acoustic center to the other. To get a full three-dimensional estimate of the intensity, the *p-p* technique has since been developed for use with probes consisting of four or more microphones. The three-dimensional particle velocity estimated by such probes can also be used to calculate energy density. In this work these probes are called multimicrophone probes. They are elsewhere also referred to as vector probes, intensity probes, and energy density sensors. Multimicrophone probe arrangements that have been studied are the four-microphone regular tetrahedral design shown in Fig. 1(a),[9–12] the six-microphone design shown in Fig. 1(c),[13–15] and the four-microphone orthogonal design shown in Fig. 1(e).[16,17] Typically, scattering of the sound field being measured by the probe has been avoided by making the fixture holding the microphones as small as possible.[11,18] Alternatively, microphones have been mounted on the surface of a hard sphere, making the scattering more predictable and possibly beneficial.[14,19,20] Such "spherical probes" are illustrated in Figs. 1(b), 1(d), and 1(f). This work is an analysis of the bias associated with these six probe designs in estimating intensity using the *p-p* technique.

Even for multimicrophone probes with perfectly phase and amplitude matched point sensors, the usable bandwidth is limited due to bias in the finite-sum and finite-difference approximations inherent in the *p-p* technique. This bias is dependent on the probe design and implementation. Design factors include the number of microphones used, the arrangement of the microphones relative to each other, and the design of the fixture holding the microphones. Implementation factors include how the probe is oriented in the sound field and how the pressure signals recorded by the

[a)]Author to whom correspondence should be addressed. Electronic mail: curtis.wiederhold@gmail.com

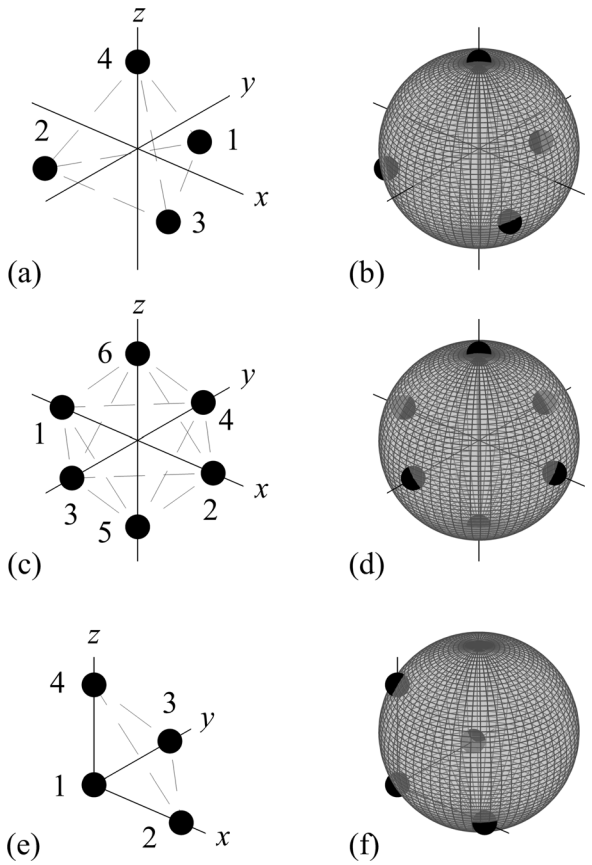


FIG. 1. Probe designs for the regular tetrahedral (a), six-microphone (c), and orthogonal (e) probes and the corresponding designs (b), (d), and (f) with microphones embedded on the surface of a hard sphere. Dots represent microphone locations.

microphones are processed to calculate intensity or energy density.

This paper compares the measurement bias of multimicrophone probes consisting of perfect point sensors in plane wave fields. It furthers the work of Pascal and Li[21] and Iino *et al.*[22] by examining new probe implementations, exploring the effect of having the microphones mounted on a rigid sphere, and using a spatial average bias metric in addition to examining the maximum biases. The results from a companion paper that investigated orthogonal probes[23] are here compared to results from regular tetrahedral and six-microphone probes.

Section II develops the processing methods used by the regular tetrahedral and six-microphone probes—the processing methods of the orthogonal probe having already been described in the companion paper. Section III gives the cross-spectral formulas associated with these processing methods, Sec. IV describes the numerical model used for comparison, Sec. V gives the results of the comparison, Sec. VI describes how the numerical results compare to experimental data, and Sec. VII consists of concluding remarks.

## II. INTENSITY ESTIMATION METHODS

Letting $p$ be the complex pressure and $\mathbf{v}$ the complex particle velocity vector, the active acoustic intensity is given by

$$\mathbf{I} = \frac{1}{2}\mathrm{Re}\{p\mathbf{v}^*\}, \tag{1}$$

where the asterisk denotes the complex conjugate and "Re" denotes the real part. With a multimicrophone probe there is more than one way to estimate this quantity, mainly arising from the various ways the pressure can be estimated. These processing methods will be explained for the regular tetrahedral and the six-microphone probes.

### A. Regular tetrahedral probe estimation methods

The regular tetrahedral probe consists of four microphones located at the vertices of a tetrahedron whose faces are all equilateral triangles. In this arrangement all the microphones are equidistant from each other. The microphones of this probe have either been implemented in a "freely suspended"[24] fashion as illustrated in Fig. 1(a) or mounted on the surface of a hard sphere[25] as illustrated in Fig. 1(b).

The particle velocity can be obtained using the time-harmonic linear Euler's equation (using the $e^{j\omega t}$ time convention),

$$\mathbf{v} = \frac{j\nabla p}{\rho\omega}, \tag{2}$$

where $j$ is $\sqrt{-1}$, $\rho$ is the density of the fluid, and $\omega$ is the angular frequency. The gradient of the pressure is estimated by a finite-difference approximation using the systematic method developed by Pascal and Li.[21] It is dependent on the location of the microphones in the coordinate system and for the configuration shown in Figs. 1(a) and 1(b) is given by

$$\mathbf{v} = \begin{cases} v_x \approx \dfrac{\sqrt{6}j(p_3 - p_2)}{4a\rho\omega} \\ v_y \approx \dfrac{\sqrt{2}j(2p_1 - p_2 - p_3)}{4a\rho\omega} \\ v_z \approx \dfrac{j(3p_4 - p_1 - p_2 - p_3)}{4a\rho\omega}, \end{cases} \tag{3}$$

where $p_i$ is the pressure at the $i$th microphone and $a$ is the radius of the sphere that is circumscribed by the four microphones. The other needed quantity in Eq. (1) is the pressure $p$ and is typically approximated as the mean of the four microphones,

$$p \approx \frac{p_1 + p_2 + p_3 + p_4}{4}. \tag{4}$$

However, it is unclear what the effect would be if instead the pressure from a single microphone were used. As a single-microphone pressure estimate leads to low intensity magnitude bias for the orthogonal probe,[23] this pressure estimate is examined in this paper and is given by

$$p \approx p_1. \tag{5}$$

The two pressure estimates combined with the consideration of whether to have the microphones embedded on the surface of a sphere or not lead to four combinations of the regular tetrahedral probe that will be analyzed.

### B. Six-microphone probe estimation methods

The six-microphone probe consists of six microphones arranged along the three Cartesian axes and can be freely suspended[13] as in Fig. 1(c) or mounted on the surface of a hard sphere[14] as in Fig. 1(d). It was suggested as an alternative to the four-microphone probes as its traditional use only requires each pair of microphones to be matched (as opposed to four matched microphones) to get an accurate measurement. This is because, in the traditional use, the intensity in each Cartesian direction is estimated using only the two microphones along that axis. The six-microphone probe design is also easier to orient in a sound field than the regular tetrahedral probe as each two-microphone pair lies along an orthogonal axis. Having three matched pairs allows a measurement of the three orthogonal components of the intensity vector. For example, the $x$-direction intensity is estimated as

$$I_x \approx \frac{1}{2}\mathrm{Re}\left\{\frac{p_1+p_2}{2}v_x^*\right\}. \tag{6}$$

The pressure estimate for this component of the intensity is the average pressure of the two microphones along the $x$ axis. The $y$- and $z$-intensities are calculated similarly, using only the two microphones along each axis. Unlike the regular tetrahedral probe where only one global pressure value is used, there is a different pressure estimate for the $x$-, $y$-, and $z$-directions.

Pascal and Li[21] showed that substantially less bias results for the six-microphone probe in measuring intensity if just one pressure estimate is used for all orthogonal directions and is given as the average of the pressures of all six microphones:

$$p \approx \frac{p_1+p_2+p_3+p_4+p_5+p_6}{6}. \tag{7}$$

This method nominally requires that all six microphones be matched for an accurate measurement, though, as microphone design has improved, matching is less of a concern today. A third considered pressure estimate is examined where the pressure from just one microphone is used:

$$p \approx p_1. \tag{8}$$

Microphone one is used here but using any other microphone gives equivalent results in this analysis due to the symmetry of the problem. This pressure estimate also nominally requires all six microphones to be matched.

The particle velocity can be calculated using Euler's equation as before. The needed pressure gradient is again calculated using a finite-difference estimate resulting in

$$\mathbf{v} = \begin{cases} v_x \approx \dfrac{j(p_2-p_1)}{2a\rho\omega} \\ v_y \approx \dfrac{j(p_4-p_3)}{2a\rho\omega} \\ v_z \approx \dfrac{j(p_6-p_5)}{2a\rho\omega}. \end{cases} \tag{9}$$

Another method to estimate intensity using the six-microphone probe was developed by Moschioni *et al.*[26] The typical velocity estimate given in Eq. (9) results in using just the microphone pairs that lie along the three orthogonal directions, even though there are a total of 15 microphone pairs in a six-microphone probe. The other 12 pairs have a microphone separation distance that is smaller than that of the three on-axis pairs by a factor of $\sqrt{2}$. This smaller separation distance extends the upper limit in using a finite-difference approximation. They thus suggest that all microphone pairs in the six-microphone probe be used to estimate the intensity, using an averaging procedure to weigh the contributions from each microphone pair. A finite-sum pressure estimate and a finite-difference velocity estimate between each microphone pair results in 15 intensity estimates. Each of these estimates is a component of the full vector intensity along the line from the first microphone in the pair to the second. These 15 intensities are averaged with frequency-dependent weighting factors $\alpha$ and $\beta$ according to

$$\mathbf{I} = \begin{cases} I_x \approx \alpha I_{12} + \beta A_1 \\ I_y \approx \alpha I_{34} + \beta A_2 \\ I_z \approx \alpha I_{56} + \beta A_3, \end{cases} \tag{10}$$

with

$$\begin{aligned} A_1 &= I_{13}+I_{14}+I_{15}+I_{16}+I_{32}+I_{42}+I_{52}+I_{62}, \\ A_2 &= I_{31}+I_{32}+I_{35}+I_{36}+I_{14}+I_{24}+I_{54}+I_{64}, \\ A_3 &= I_{51}+I_{52}+I_{53}+I_{54}+I_{16}+I_{26}+I_{36}+I_{46}, \end{aligned} \tag{11}$$

where $I_{ij}$ is the intensity component along the line from microphone $i$ to microphone $j$ and $\alpha$ and $\beta$ are given by

$$\alpha = \frac{\sin^2\left(\dfrac{2a\omega}{c}\right)}{4\sin^2\left(\dfrac{2a\omega}{\sqrt{2}c}\right)+\sin^2\left(\dfrac{2a\omega}{c}\right)} \quad \text{and}$$

$$\beta = \frac{\sin^2\left(\dfrac{2a\omega}{\sqrt{2}c}\right)}{4\sqrt{2}\sin^2\left(\dfrac{2a\omega}{\sqrt{2}c}\right)+\sqrt{2}\sin^2\left(\dfrac{2a\omega}{c}\right)}, \tag{12}$$

where $c$ is the sound speed. This procedure was found by Moschioni *et al.*[26] to considerably increase the usable bandwidth of the six-microphone probe and so will be included here. This method cannot be implemented for use with the regular tetrahedral probe as the separation distance between all microphones is the same. It is also not considered for use with the orthogonal probe because the separation distance of the off-axis microphone pairs is larger than that of the on-axis pairs.

In summary, four processing methods for the six-microphone probe are examined. First, using it as three one-dimensional probes; second, using the average pressure of the six microphones; third, using microphone one for the pressure estimate; and fourth, using all microphone pairs and averaging the resulting components of the intensity. These four methods, along with the design consideration of whether or not to embed the microphones on the surface of a

sphere, account for the eight permutations of the six-microphone probe that are included in this analysis.

### C. Summary of estimation methods

For simplification an abbreviation scheme is used to refer to each probe type. The regular tetrahedral probe is abbreviated as "4R" and the six-microphone probe as "6." If the microphones of the probe are mounted on the surface of a sphere, the abbreviation "S" is used. The pressure estimate is abbreviated as the number of microphones averaged for the estimate: "1" if one microphone is used, etc. When the six-microphone probe is used as three one-dimensional probes, the abbreviation "3-1D" is used. When the average intensity of all 15 microphone pairs is used the abbreviation is given as "15-1D." A forward slash is used to separate the abbreviations dealing with the probe design from ones that concern data processing. Table I gives a summary of these probes and processing methods.

Results for the regular tetrahedral and six-microphone probes are compared to the results given in the companion paper for orthogonal probes. Abbreviations used in this paper for orthogonal probes are as given in that work with the extra abbreviation "4O" denoting the four-microphone orthogonal probe.

## III. CROSS-SPECTRAL FORMULATIONS

Calculating intensity using the *p-p* technique in practice is most commonly done in terms of auto- and cross-correlations between microphone signals. The cross-spectral expressions for all probe types listed in Table I are given, including some already given in Pascal and Li.[21] They are all given here for completeness. The one-sided cross-spectral density for a zero-mean process is defined as

$$G_{mn}(\omega) = C_{mn}(\omega) + jQ_{mn}(\omega) = \lim_{T\to\infty}\frac{2}{T}\mathrm{E}\left[P_m^*(\omega,T)P_n(\omega,T)\right], \quad (13)$$

for $\omega \geq 0$, where $C$ and $Q$ are, respectively, the real and imaginary parts of the cross-spectral density $G$. The expectation operator is denoted by E[] and $P_m$ and $P_n$ are the Fourier transforms of the pressures from the $m$th and $n$th microphones over time $T$. The equations are given for probes consisting of freely suspended microphones. If instead the intensity is to be calculated for probes consisting of microphones embedded on a sphere, the radius $a$ should be multiplied by 3/2 as shown by Elko.[19] For example, the expression for probe type 4R.S/1 is the same as that for probe type 4R/1 with $\frac{3}{2}a$ substituted for $a$. As these expressions are specific to the particular microphone numbering system and orientation of the probe in the coordinate system, they are only valid for the probes as defined in Fig. 1. Though not explicitly written in the following equations for brevity, all cross-spectral densities are functions of angular frequency. The expression for probe type 4R/1 is given by

$$\mathbf{I}_{4R/1} = \begin{cases} I_x \approx \dfrac{\sqrt{6}}{4a\rho\omega}(-Q_{21}+Q_{31}) \\ I_y \approx \dfrac{\sqrt{2}}{4a\rho\omega}(-Q_{21}-Q_{31}) \\ I_z \approx \dfrac{1}{4a\rho\omega}(-Q_{21}-Q_{31}+3Q_{41}). \end{cases} \quad (14)$$

4R/4 is given by

$$\mathbf{I}_{4R/4} = \begin{cases} I_x \approx \dfrac{\sqrt{6}}{16a\rho\omega}(-Q_{21}+Q_{31}+2Q_{32}+Q_{42}-Q_{43}) \\ I_y \approx \dfrac{\sqrt{2}}{16a\rho\omega}(-3Q_{21}-3Q_{31}-2Q_{41}+Q_{42}+Q_{43}) \\ I_z \approx \dfrac{1}{4a\rho\omega}(Q_{41}+Q_{42}+Q_{43}). \end{cases} \quad (15)$$

6/1 is given by

TABLE I. Summary of considered probe types and their abbreviations.

| Abbreviation | Probe type | Scattering | Pressure estimate |
|---|---|---|---|
| 4R/1 | Reg. tetrahedral | None | $p = p_1$ |
| 4R/4 | Reg. tetrahedral | None | $p = \frac{p_1+p_2+p_3+p_4}{4}$ |
| 4R.S/1 | Reg. tetrahedral | Spherical | $p = p_1$ |
| 4R.S/4 | Reg. tetrahedral | Spherical | $p = \frac{p_1+p_2+p_3+p_4}{4}$ |
| 6/1 | Six-microphone | None | $p = p_1$ |
| 6/6 | Six-microphone | None | $p = \frac{p_1+p_2+p_3+p_4+p_5+p_6}{6}$ |
| 6/3-1D | Six-microphone | None | $p_x = \frac{p_1+p_2}{2}$, $p_y = \frac{p_3+p_4}{2}$, $p_z = \frac{p_5+p_6}{2}$ |
| 6/15-1D | Six-microphone | None | 15 pressure estimates |
| 6.S/1 | Six-microphone | Spherical | $p = p_1$ |
| 6.S/6 | Six-microphone | Spherical | $p = \frac{p_1+p_2+p_3+p_4+p_5+p_6}{6}$ |
| 6.S/3-1D | Six-microphone | Spherical | $p_x = \frac{p_1+p_2}{2}$, $p_y = \frac{p_3+p_4}{2}$, $p_z = \frac{p_5+p_6}{2}$ |
| 6.S/15-1D | Six-microphone | Spherical | 15 pressure estimates |

$$\mathbf{I}_{6/1} = \begin{cases} I_x \approx \dfrac{1}{2a\rho\omega}(Q_{21}) \\ I_y \approx \dfrac{1}{2a\rho\omega}(-Q_{31} + Q_{41}) \\ I_z \approx \dfrac{1}{2a\rho\omega}(-Q_{51} + Q_{61}). \end{cases} \tag{16}$$

6/6 is given by

$$\mathbf{I}_{6/6} = \begin{cases} I_x \approx \dfrac{B_1}{12a\rho\omega} \\ I_y \approx \dfrac{B_2}{12a\rho\omega} \\ I_z \approx \dfrac{B_3}{12a\rho\omega}, \end{cases} \tag{17}$$

where

$$\begin{aligned} B_1 &= 2Q_{21} + Q_{31} - Q_{32} + Q_{41} - Q_{42} \\ &\quad + Q_{51} - Q_{52} + Q_{61} - Q_{62}, \\ B_2 &= -Q_{31} - Q_{32} + Q_{41} + Q_{42} + 2Q_{43} \\ &\quad + Q_{53} - Q_{54} + Q_{63} - Q_{64}, \\ B_3 &= -Q_{51} - Q_{52} - Q_{53} - Q_{54} + Q_{61} \\ &\quad + Q_{62} + Q_{63} + Q_{64} + 2Q_{65}. \end{aligned} \tag{18}$$

6/3-1D is given by

$$\mathbf{I}_{6/3-1\mathrm{D}} = \begin{cases} I_x \approx \dfrac{Q_{21}}{2a\rho\omega} \\ I_y \approx \dfrac{Q_{43}}{2a\rho\omega} \\ I_z \approx \dfrac{Q_{65}}{2a\rho\omega}. \end{cases} \tag{19}$$

The expressions for the 15-1D probe types are given as the average of intensities from all two-microphone pairs of the probe. The intensity between any two microphones $i$ and $j$ is estimated as

$$\mathbf{I}_{ij} \approx \frac{Q_{ji}}{d\rho\omega}, \tag{20}$$

where $d$ is the distance between the two microphones ($d = 2a$ for three of the microphone pairs and $d = \sqrt{2}a$ for the other 12 microphone pairs). These intensities are then averaged according to Eqs. (10) and (12).

## IV. COMPARISON MODEL

A numerical model of the probes with matched point sensors in a plane wave field is used to compare the bias of each probe type. The angle of incidence of the plane wave field on the probe affects the probe's accuracy and so multiple angles of incidence must be considered. A step size of $\pi/50$ in the $\theta$ and $\varphi$ spherical directions of the angle of incidence is seen to be sufficient to calculate the metrics used for comparison.

Three metrics are used for probe comparison and are plotted for each probe as a function of dimensionless frequency. The metrics are ways of summarizing the different amounts of bias at different angles of incidence into a single value at each frequency. The first is maximum bias, which corresponds to the angle of incidence that results in the most measurement error. If a probe were oriented randomly in a plane wave field, this metric would give a bound to the largest measurement bias that would be expected. The second metric is root-mean-square (rms) bias. This metric represents the amount of bias as a function of frequency that could be expected on average if a probe were randomly oriented in a plane wave field. Third, bias spread—the difference between the maximum and minimum bias—is examined. This metric is an indication of how well the probe can be corrected for intensity magnitude with better calibration possible if the spread is smaller. The use of such correction factors is discussed further in Sec. V. The first two metrics are used in analyzing bias for both intensity magnitude and direction, while the third metric is used only for intensity magnitude.

The intensity direction bias is defined to be the angle (in degrees) between the angle of incidence of the incoming plane wave and the angle estimated by the probe measurement. The equation for this is

$$I_{\mathrm{dir\,err}\,(\theta_i,\varphi_j)} = \frac{180}{\pi}\cos^{-1}\left(\frac{\mathbf{I}_{\mathrm{est}(\theta_i,\varphi_j)} \cdot \mathbf{I}_{\mathrm{exact}}}{\|\mathbf{I}_{\mathrm{est}(\theta_i,\varphi_j)}\|\|\mathbf{I}_{\mathrm{exact}}\|}\right), \tag{21}$$

where the dot product between $\mathbf{I}_{\mathrm{est}(\theta_i,\varphi_j)}$, the estimated intensity vector at incidence angle $(\theta_i,\varphi_j)$, and $\mathbf{I}_{\mathrm{exact}}$, the actual intensity, is taken and then divided by the magnitudes of the two vectors. The intensity magnitude bias is given in dB and defined as follows:

$$I_{\mathrm{mag\,err}\,(i,j)} = 10\log\frac{\|\mathbf{I}_{\mathrm{est}(\theta_i,\varphi_j)}\|}{\|\mathbf{I}_{\mathrm{exact}}\|}. \tag{22}$$

To calculate the rms bias the values are then squared and multiplied by an appropriate weighting function to convert the results from an equal angle approach arising from using a constant step size in the $\theta$ and $\varphi$ coordinates to an equal area approach that is appropriate for calculating the average bias.[27,28] The square root is then taken of the mean of the weighted, squared values.[23]

This work considers probes with microphones either mounted on a hard sphere or freely suspended in space. In the sphere-mounted case, spherical scattering is accounted for using 25 terms of a series expansion;[29] however, scattering off any fixture holding the sphere is neglected. In the case of freely suspended microphones, scattering is neglected entirely. Because of this, it could be expected that the results from the simulation will match experimental results more closely for the spherical probes than for the freely suspended probes.

The spherical scattering has been shown to effectively increase the separation distance between microphones at low frequencies and so the 3/2 correction factor must be used as mentioned earlier for the finite-difference expressions to give accurate results. Results for freely suspended probes are plotted as a function of the dimensionless frequency $ka$

where $k$ is the wavenumber and $a$ is the radius of an imaginary sphere that is circumscribed by the four microphone points. However, for spherical probes, the bias is plotted as a function of $\frac{3}{2}ka$ where $a$ is the radius of the sphere on which the microphones are mounted. The result is that, because of the needed correction factor, the spherical probe is directly compared to a freely suspended probe that is 3/2 times larger, an approach used by both Elko[19] and Parkins *et al.*[14] Hence, the bias at any frequency $ka$ of a freely suspended probe are directly compared to the bias at $\frac{3}{2}ka$ for a spherical probe. Results are given up to $ka = 1.5$ for freely suspended probes and $\frac{3}{2}ka = 1.5$ ($ka = 1$) for spherical probes.

## V. RESULTS AND DISCUSSION

### A. Regular tetrahedral probe results

The regular tetrahedral probe is examined first—bias in estimating intensity magnitude is shown in Fig. 2 and intensity direction in Fig. 3. In the following figures the top two plots, (a) and (b), show rms bias and the bottom two, (c) and (d), the maximum bias. The left plots, (a) and (c), are for probes with microphones freely suspended in space (no scattering) while the right plots, (b) and (d), show bias for spherical probes (spherical scattering).

Figures 2(a) and 2(b) show that using either the pressure from one microphone or the average pressure of all microphones results in similar intensity magnitude bias averaged over angle of incidence. However, Figs. 2(c) and 2(d) show that a higher maximum bias is seen when using the pressure from one microphone. Comparing the left and right graphs

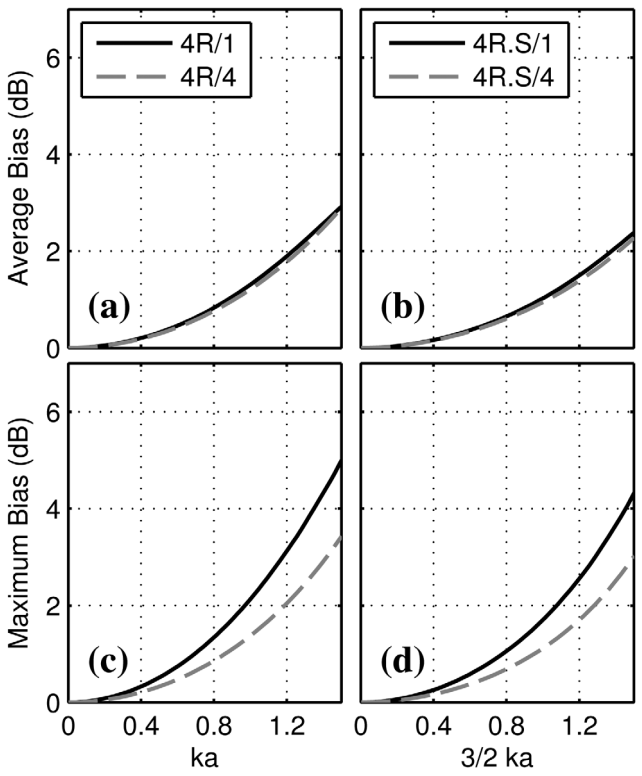


FIG. 2. RMS intensity magnitude bias for freely suspended (a) and spherical (b) regular tetrahedral probe types and corresponding maximum bias (c) and (d).

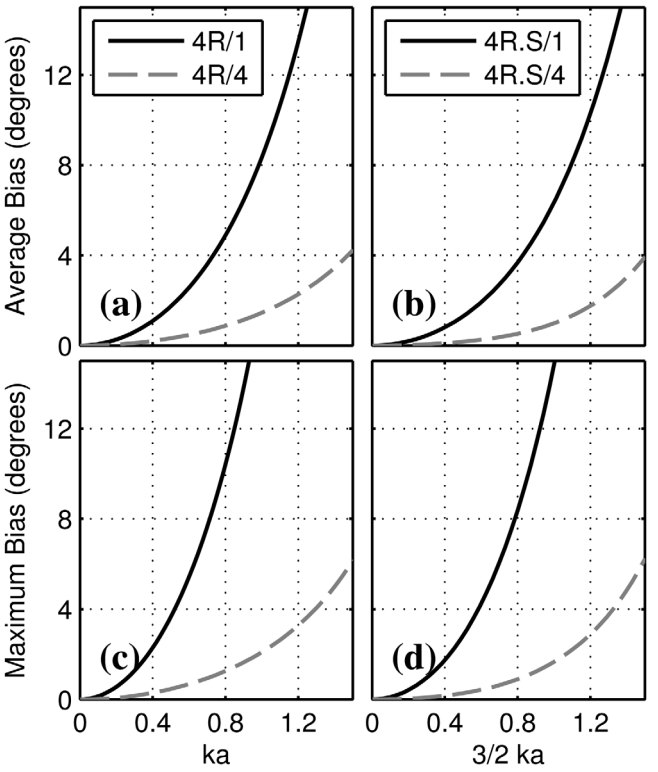


FIG. 3. RMS intensity direction bias for freely suspended (a) and spherical (b) regular tetrahedral probe types and corresponding maximum bias (c) and (d).

shows that in this case mounting the microphones in a sphere results in a slightly lower bias.

For intensity direction, Fig. 3 indicates that the one-microphone pressure estimate gives a significantly worse average and maximum results than using the average of the four microphones. The results for the spherical probe are similar to those for the freely suspended probe.

### B. Six-microphone probe results

The six-microphone probe results are shown in Figs. 4 and 5. For this probe, the best results are shown to come from the method of averaging intensity estimates from all 15 microphone pairs (6/15-1D and 6.S/15-1D). Introducing spherical scattering results in a lower bias in all cases.

The results for 6/1 and 6/3-1D are exactly equivalent up to $ka = \pi/2$ for the intensity magnitude maximum bias shown in Fig. 4(c). Maximum bias for both probes up to that frequency occurs for incoming waves in the $+x$ and $-x$ directions, the axis that microphone one lies on. At these directions there are no $x$- or $z$-components of the intensity estimate and it can be shown that the expression for the $x$-component for 6/1 reduces to that of 6/3-1D. The results for their spherical counterparts (6.S/1 and 6.S/3-1D), seen in Fig. 4(d), show a similar equivalence, but up to $\frac{3}{2}ka \approx 1.66$. The diverging error in both cases is due to errors in the finite-sum approximations. In the case of no scattering this error diverges when a half wavelength is equal to the diameter of the probe, the distance between microphones one and two.[18,30] With spherical scattering, the build up of pressure on the incidence side of the sphere offsets the finite-sum

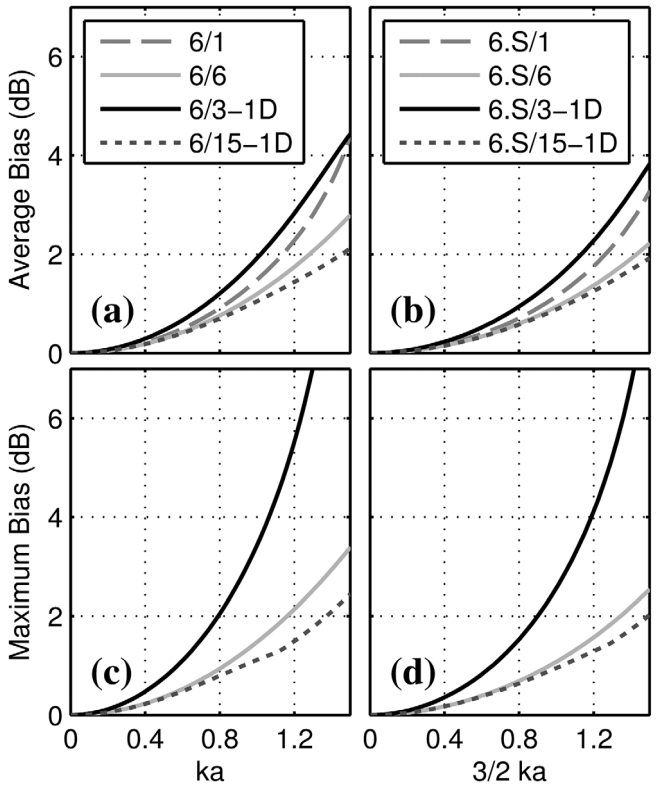


FIG. 4. RMS intensity magnitude bias for freely suspended (a) and spherical (b) six-microphone probe types and corresponding maximum bias (c) and (d).

errors and shifts this critical frequency out some. At these critical frequencies the direction of the intensity estimate is exactly opposite of the true direction, making the maximum biases plotted in Figs. 5(c) and 5(d) jump to 180°.

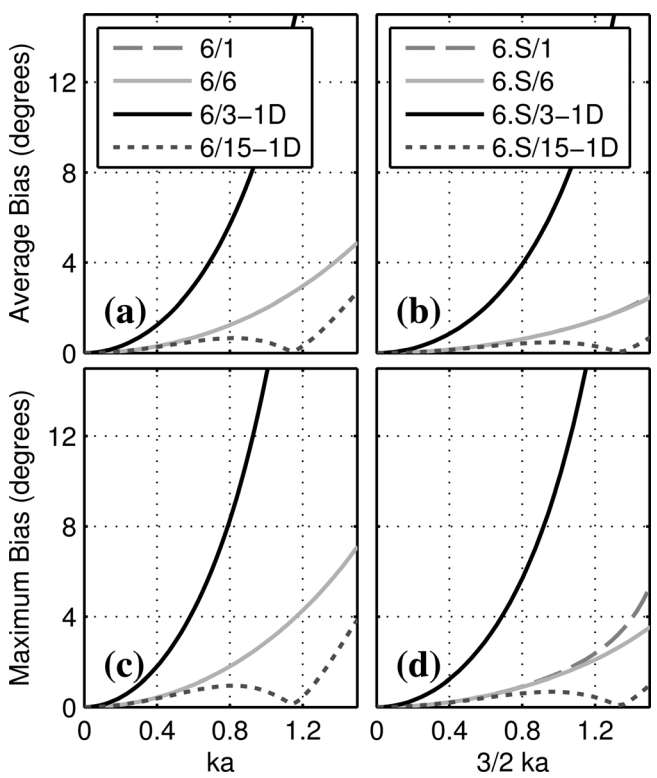


FIG. 5. RMS intensity direction bias for freely suspended (a) and spherical (b) six-microphone probe types and corresponding maximum bias (c) and (d).

For maximum direction bias overlap is now seen between 6/1 and 6/6. In this case the equivalence is more complicated, not restricted to a single angle of incidence, but due to the symmetry of the problem. As shown in Figs. 5(b) and 5(d) spherical scattering breaks this equivalence at higher frequencies.

### C. Comparison of probe geometries

A comparison of the probe geometries is made by looking at the lowest-bias processing method of each. For the regular tetrahedral geometry both 4R/1 and 4R/4 show nearly equal amounts of rms average bias; however, 4R/4 has a lower maximum bias and so is used for the probe geometry comparison. The lowest-bias processing method for the six-microphone geometry is to use all 15 intensities (6/15-1D and 6.S/15-1D). Previous work[23] shows that for the orthogonal geometry the lowest intensity magnitude bias results from using the pressure of the origin microphone and a three-point velocity estimate (abbreviated in that paper as 1.3 and S/1.3 and given the additional 4O abbreviation in this paper) and, for intensity direction, a Taylor expansion pressure and velocity estimate (T.T and S/T.T). These lowest-bias processing methods for each probe geometry are compared for intensity magnitude in Fig. 6 and intensity direction in Fig. 7.

The orthogonal probe types (4O/1.3 and 4O.S/1.3) are shown in Fig. 6 to measure the intensity magnitude the most accurately by a dB or so at the highest frequency considered. However, in Fig. 7, the six-microphone probe is shown to be more accurate for intensity direction. Comparing the left and

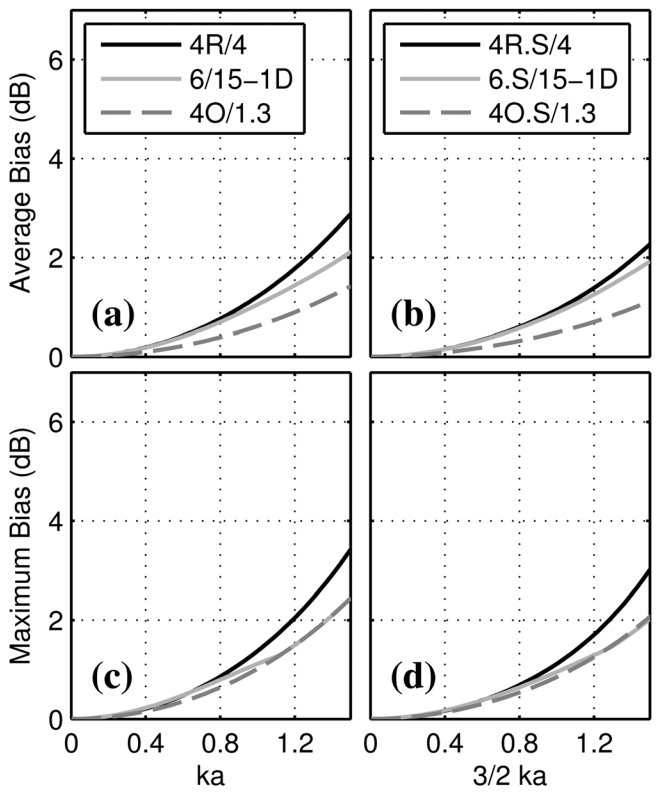


FIG. 6. RMS intensity magnitude bias for the lowest-bias freely suspended (a) and spherical (b) probe types and corresponding maximum bias (c) and (d).

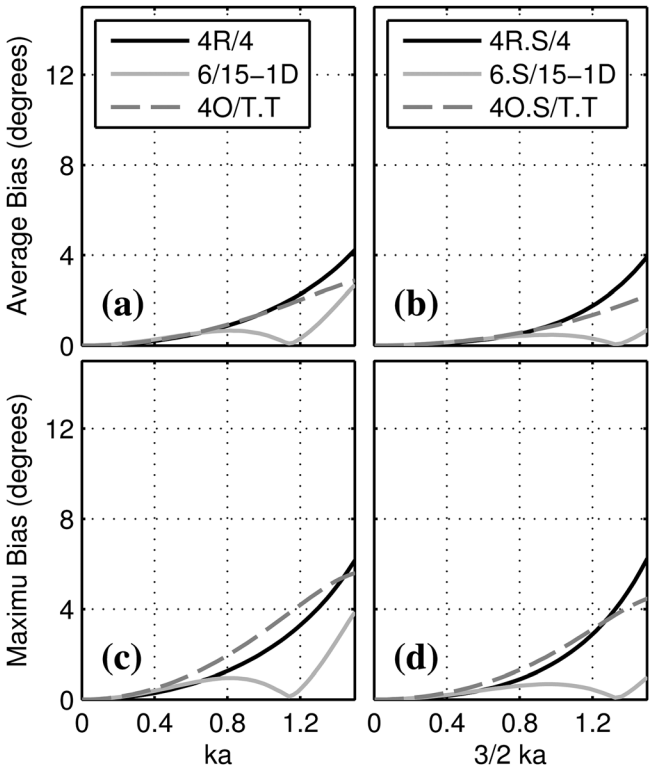


FIG. 7. RMS intensity direction bias for the lowest-bias freely suspended (a) and spherical (b) probe types and corresponding maximum bias (c) and (d).

right graphs in these figures shows spherical designs exhibiting less bias than their freely suspended counterparts.

These results compare the probe geometries for the *p-p* processing methods currently found in the literature. It should be noted that the comparison could change if other *p-p* processing methods were to be developed.

### D. Effect of mounting microphones in sphere

To analyze more directly the effect of the spherical scattering the difference in bias between each spherical design and its corresponding freely suspended design is given in Table II. The bias values reported are only for the highest frequency considered. This serves as a general indication of the bias at all lower frequencies since the bias curves all follow a similar monotonically increasing trend (probe type 6/15-1D being an exception). A positive value indicates that the spherical design results in more bias than its freely suspended counterpart. For example, the first row of the table shows that mounting the microphones in a sphere leads to 0.54 dB less rms average bias in estimating intensity magnitude with probe type 4R/1 at the highest frequency considered. The results show that spherical designs exhibit a lower rms average bias for intensity magnitude and direction and, except 4R/4, have less intensity magnitude bias spread.

TABLE II. Bias difference between spherical and freely suspended probe designs at the highest frequency considered.

| Probe type | Magnitude bias (dB) | Magnitude bias spread (dB) | Direction bias (degrees) |
|---|---|---|---|
| 4R.S/1—4R/1 | −0.54 | −0.36 | −5.85 |
| 4R.S/4—4R/4 | −0.62 | 0.02 | −0.30 |
| 6.S/1—6/1 | −1.12 | −4.22 | −2.35 |
| 6.S/6—6/6 | −0.57 | −0.42 | −2.44 |
| 6.S/3-1D—6/3-1D | −0.61 | −3.98 | −10.34 |
| 6.S/15-1D—6/15-1D | −0.20 | −0.43 | −1.99 |

### E. Summary of lowest-bias probe types

A summary of the ten lowest-bias probe types for intensity magnitude, magnitude spread, and direction is given in Table III. The rms bias of each probe at the highest frequency considered is given in parentheses. Table III shows that for intensity magnitude the lowest bias is achieved with the orthogonal probe types. However, the intensity magnitude bias spread is lowest for the six-microphone probe types. For intensity direction, 6.S/15-1D exhibits the lowest bias and 4O.S/T.T the next lowest.

### F. Correction factors

Bearing in mind the assumptions made in this analysis, the biases calculated here could be used as correction factors to calibrate the probes for intensity magnitude. An important consideration in applying such correction factors, and thus in the merit of any particular probe, is the spread between the maximum and minimum intensity magnitude bias over the angle of incidence. The smaller the spread, the more effective the correction factors will be. There are two ways the correction factors could be computed. First, they could be calculated as the mean of the maximum and minimum bias. This would effectively make the new maximum bias at any frequency equal to one-half the value of the bias spread. Alternatively, they could be calculated as the rms average biases as shown in the plots of this paper. Correcting to these values results in less bias on average if the probe were randomly oriented in a sound field; however, there would exist angles of incidence where the maximum bias would be more than one-half the value of the bias spread.

It may also be possible for probes to be corrected for intensity direction, but the bias would have to be known in terms of the $\theta$ and $\varphi$ spherical angles as opposed to merely the angle between the actual and estimated intensity vectors (which is what is reported in this work). Also, for the correction to be effective there would need to be a one-to-one

TABLE III. Ten lowest-bias probe types for each quantity of interest. RMS bias at highest frequency considered given in parentheses.

| Rank | Magnitude bias (dB) | Magnitude bias spread (dB) | Direction bias (degrees) |
|---|---|---|---|
| 1 | 4O.S/1.3 (1.12) | 6.S/15-1D (0.21) | 6.S/15-1D (0.68) |
| 2 | 4O/1.3 (1.42) | 6.S/6 (0.52) | 4O.S/T.T (2.20) |
| 3 | 4O.S/W.3 (1.52) | 6/15-1D (0.64) | 6.S/6 (2.44) |
| 4 | 4O.S/A.3 (1.78) | 4O.S/W.T (0.88) | 6.S/1 (2.53) |
| 5 | 4O.S/W.T (1.85) | 6/6 (0.94) | 4O.S/A.T (2.64) |
| 6 | 4O/W.3 (1.90) | 4R/4 (0.98) | 6/15-1D (2.67) |
| 7 | 4O.S/A.T (1.91) | 4R.S/4 (1.00) | 4O.S/W.T (2.79) |
| 8 | 6.S/15-1D (1.92) | 4O/1.3 (1.69) | 4O/T.T (2.87) |
| 9 | 6/15-1D (2.12) | 4O/W.T (1.70) | 4O.S/1.T (3.25) |
| 10 | 4O/W.T (2.17) | 4O/W.3 (1.95) | 4O/A.T (3.89) |

correspondence between each actual angle of incidence and estimated angle of incidence. That is, if one estimated angle of incidence corresponded to more than one actual angle of incidence, an accurate correction would not be possible without more information. If an intensity direction correction were possible, a more accurate intensity magnitude correction could also then be applied that was specific to the corrected angle of incidence. The general idea of using direction information to correct intensity magnitude has been examined by Suzuki *et al.*[31] and Iino *et al.*[22]

### G. Definition of *kd*

Results given in this paper and similar analyses[14,21,23] are largely dependent on the choice of the length $d$ in the dimensionless frequency $kd$. In the analysis done by Pascal and Li,[21] this distance for the regular tetrahedron is chosen to be the distance between any two microphones, for the six-microphone probe it is the distance between any two microphones that lie on the same axis, and for the orthogonal probe it is the distance between the "origin" microphone and any of the other three microphones. As the distances in this paper are chosen differently, results reported differ accordingly. The frequency axis of the bias plots is scalable depending on how the dimensionless frequency is defined. While this approach gives an indication of the relative merit of any particular probe design, it is not general because of its dependence on the arbitrary definition of $d$ for each probe geometry.

If phase mismatch were introduced into the comparisons, the definition of the distance $d$ could become less important. Adding in phase mismatch introduces low-frequency bias because the phase error becomes large relative to the acoustic phase change between microphones due to the larger wavelengths. For example, two microphones separated by 3 cm measure a 65 Hz tone with about a 2° phase difference. Therefore, a 1° phase mismatch between the two microphones would introduce large bias into the measurement; whereas, at 3500 Hz, a 1° phase error is fairly negligible compared to the 110° phase difference resulting from a 3 cm separation distance. With phase mismatch introduced, any particular probe design could then have a high-frequency limit as well as a low-frequency limit where the estimation bias is greater than a chosen threshold. This is a useful way to benchmark probe designs because the frequency range between the low- and high-frequency limits is independent of the definition of the separation distance $d$. For example, suppose a particular probe design was shown to have less than 3° of bias in estimating the intensity direction between a $kd$ of 0.2 to 2 while another design was only able to meet the criteria from a $kd$ of 0.2 to 1. In the first case, the high-frequency cutoff was 10 times greater than that of the low while, for the second case, it was 5 times greater. The first probe is thus shown to have a larger bandwidth than the second probe, regardless of the definition of the distance $d$. This then serves as a better indicator in comparing probe geometries.

Until this is explored further, though, the value of $d$ is chosen as it is in the present work in order to directly compare designs mounted in a sphere to those not in a sphere. For designs not mounted in a sphere, the length $d$ is chosen to be the radius of an imaginary sphere circumscribing the four or six sensors. For designs mounted in a sphere, results are plotted using the length $\frac{3}{2}a$ where $a$ is the radius of the actual sphere.

## VI. EXPERIMENTAL VERIFICATION

Experimental results help validate the numerical results and show what limitations might be found in practice. Three-dimensional acoustic intensity was measured using the four-microphone probe shown in Fig. 8. Four microphones are flush-mounted on the surface of a 2.54 cm (1 in.) diameter sphere. The lower three microphones are equally spaced in a plane at a 60° angle to the line formed from any of these microphones to the microphone on top of the sphere. This makes it nearly a regular tetrahedron, for which this angle is instead 54.7° [$\cos^{-1}(1/\sqrt{3})$]. The probe was oriented vertically and recorded white noise band limited from 200 to 10 000 Hz produced by a loudspeaker pointed horizontally at the probe in an anechoic chamber. The probe was mounted to a turntable and rotated 2.5° for each measurement until an entire rotation was complete for a total of 144 measurements.

The intensity was estimated using both the average pressure and the pressure from microphone one as in Eqs. (14) and (15). However, the equations needed to be modified slightly since the tetrahedron is not regular: The $x$- and $y$-intensities were multiplied by $4\sqrt{6}/9$ and the $z$-intensity by 8/9. This estimated intensity magnitude was compared to a reference intensity magnitude calculated using $p_1{}^2/\rho c$, assuming planarity of the impinging waves. The angle between the loudspeaker and the rotated probe was used as the reference intensity angle. The rms and maximum bias of the 144 measurements was then calculated for each frequency and compared to results from the numerical model. While the numerical results presented earlier were bias relative to the known intensity, for better comparison to the experiment the numerical intensity magnitude bias was instead calculated relative to the quantity $p_1{}^2/\rho c$, where $p_1$ in this case is the pressure at microphone one as calculated by the simulation to include scattering. The comparison for intensity magnitude is shown in Fig. 9 and for intensity direction in Fig. 10. A similar naming convention is used to

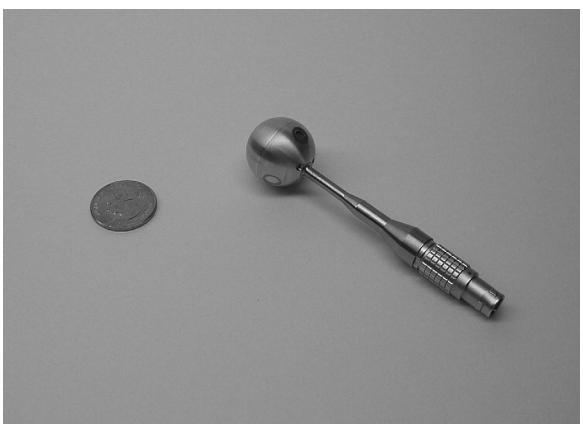

FIG. 8. Four-microphone probe used for experimental results.

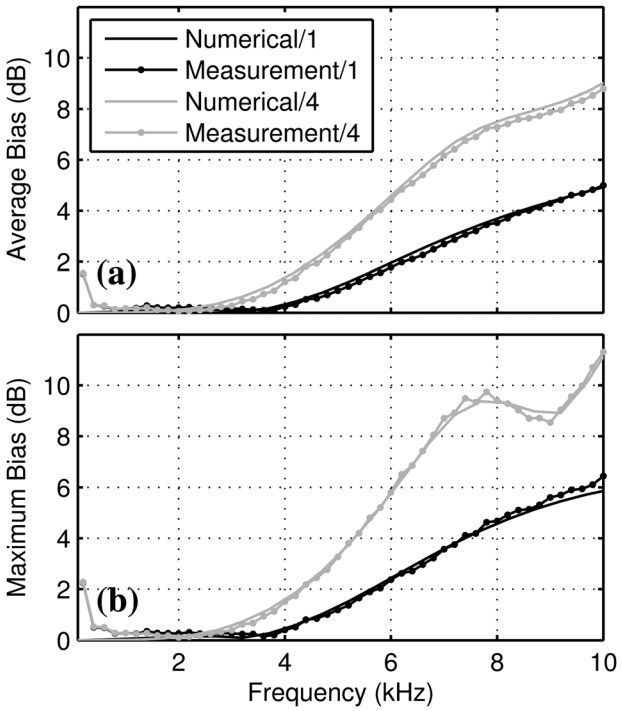


FIG. 9. Intensity magnitude bias comparison of numerical and measurement results. RMS bias (a) and maximum bias (b).

the results presented earlier: "1" indicates that the pressure estimate came from microphone one while "4" indicates that an average of the four microphones was used.

There is satisfactory agreement across most of the plotted frequency range. The numerical results generally slightly overestimate the intensity magnitude bias and underestimate, by up to 5° in the rms average, the direction bias. At low frequencies, the measured results diverge due to microphone phase mismatch.

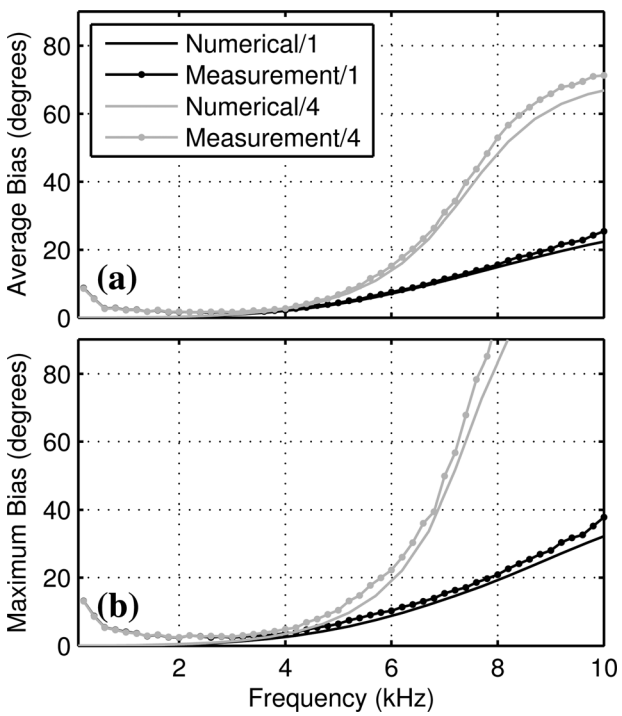


FIG. 10. Intensity direction bias comparison of numerical and measurement results. RMS bias (a) and maximum bias (b).

## VII. CONCLUSIONS

The intensity measurement bias of various configurations of multimicrophone probes was analyzed over multiple angles of incidence. It should be noted that these results are valid only for the conditions stated: Perfect point sensors, plane wave fields, with *kd* defined as it is. Under these conditions it was shown that the probe type with the lowest bias for intensity magnitude is 4O.S/1.3—the orthogonal probe with sensors mounted on a sphere, using the origin microphone for the pressure estimate. This orthogonal probe design had around 1 dB less average bias than the lowest-bias processing method for the regular tetrahedral or six-microphone designs at the highest frequency considered. However, if probes were to be corrected for intensity magnitude bias the lowest bias would come from 6.S/15-1D—the six-microphone probe using a weighted average of the 15 intensities.

Probe type 6.S/15-1D also had the least amount of direction bias. The rms average bias of this probe at the highest frequency considered was between 1° and 3° less than the lowest-bias processing methods of the other two probe geometries. Choosing one processing method over another made a more substantial difference for intensity direction than for magnitude as certain processing methods resulted in a very large direction bias.

Mounting sensors in a sphere was shown to generally give lower bias than having the sensors freely suspended regardless of probe geometry or processing method. As scattering was entirely neglected for the freely suspended case, it is expected that experimental results for spherical probes would more closely match the results presented in this paper than would experimental results for freely suspended probes. The lower bias of spherical designs was less than 2 dB for rms intensity magnitude at the highest frequency considered. For intensity direction, spherical designs showed between 0° and 10° less average bias at the highest frequency considered.

Comparisons between probe designs are highly dependent on how the distance *d* is defined in the dimensionless frequency *kd*. Future work could include introducing phase mismatch errors and comparing the probes based on the size of the bandwidth over which a probe type has less than a determined threshold level of bias. Another useful approach could consist of correcting intensity direction bias using numerical results, and then using the numerical results at the corrected angle of incidence to correct the intensity magnitude.

## ACKNOWLEDGMENT

This work was supported in part by the NASA Stennis Space Center Small Business Innovative Research program through a subcontract from Blue Ridge Research and Consulting.

[1]F. J. Fahy, "Measurement of acoustic intensity using the cross-spectral density of two microphone signals," J. Acoust. Soc. Am. **62**, 1057–1059 (1977).
[2]G. Pavic, "Measurement of sound intensity," J. Sound Vib. **51**, 533–545 (1977).

[3]J. Y. Chung, "Cross-spectral method of measuring acoustic intensity without error caused by instrument phase mismatch," J. Acoust. Soc. Am. **64**, 1613–1616 (1978).
[4]F. J. Fahy, *Sound Intensity*, 2nd ed. (E & FN Spon, London, 1995), pp. 91–97.
[5]F. Jacobsen and H. E. de Bree, "A comparison of two different sound intensity measurement principles," J. Acoust. Soc. Am. **118**, 1510–1517 (2005).
[6]H.-E. de Bree, P. Leussink, T. Korthorst, H. Jansen, T. S. J. Lammerink, and M. Elwenspoek, "The $\mu$-flown: A novel device for measuring acoustic flows," Sens. Actuators, A **54**, 552–557 (1996).
[7]E. G. Williams, N. Valdivia, and P. C. Herdic, "Volumetric acoustic vector intensity imager," J. Acoust. Soc. Am. **120**, 1887–1897 (2006).
[8]D. P. Jarrett, E. A. P. Habets, and P. A. Naylor, "3D source localization in the spherical harmonic domain using a pseudo intensity vector," in *European Signal Processing Conference (EUSIPCO)*, Aalborg, Denmark (2010).
[9]L. M. C. Santos, C. C. Rodrigues, and J. L. Bento Coelho, "Measuring the three-dimensional acoustic intensity vector with a four-microphone probe," in *Proceedings of Inter-Noise*, Newport Beach, CA (1989), pp. 965–968.
[10]R. Hickling and A. W. Brown, "Determining the direction to a sound source in air using vector sound-intensity probes," J. Acoust. Soc. Am. **129**, 219–224 (2011).
[11]H. Suzuki, S. Oguro, M. Anzai, and T. Ono, "Performance evaluation of a three dimensional intensity probe," J. Acoust. Soc. Jpn. **16**, 233–238 (1995).
[12]K. L. Gee, J. H. Giraud, J. D. Blotter, and S. D. Sommerfeldt, "Near-field vector intensity measurements of a small solid rocket motor," J. Acoust. Soc. Am. **128**, EL69–EL74 (2010).
[13]G. Rasmussen, "Measurement of vector fields," in *Proceedings of the Second International Congress on Acoustic Intensity*, Senlis, France (1985), pp. 53–58.
[14]J. W. Parkins, S. D. Sommerfeldt, and J. Tichy, "Error analysis of a practical energy density sensor," J. Acoust. Soc. Am. **108**, 211–222 (2000).
[15]S. Nagata, K. Furihata, T. Wada, D. K. Asano, and T. Yanagisawa, "A three-dimensional sound intensity measurement system for sound source identification and sound power determination by ln models," J. Acoust. Soc. Am. **118**, 3691–3705 (2005).
[16]M. Schumacher, "A transducer and processing system to measure total acoustic energy density," M.S. thesis, University of Texas at Austin, Austin, TX, 1984.
[17]B. S. Cazzolato and C. H. Hansen, "Errors arising from three-dimensional energy density sensing in one-dimensional sound fields," J. Sound Vib. **236**, 375–400 (2000).
[18]B. S. Cazzolato and C. H. Hansen, "Errors in the measurement of acoustic energy density in one-dimensional sound fields," J. Sound Vib. **236**, 801–831 (2000).
[19]G. W. Elko, "An acoustic vector-field probe with calculable obstacle bias," in *Proceedings of Noise-Con 91*, Tarrytown, NY (1991), pp. 525–532.
[20]F. Ayme, C. Cariou, M. Ichchou, and D. Juvé, "A new acoustic three dimensional intensity and energy density probe," in *Proceedings of Acoustics 2012 Nantes* (2012), pp. 2063–2068.
[21]J.-C. Pascal and J.-F. Li, "A systematic method to obtain 3D finite-difference formulations for acoustic intensity and other energy quantities," J. Sound Vib. **310**, 1093–1111 (2008).
[22]T. Iino, H. Tatekawa, H. Mizukawa, and H. Suzuki, "Numerical evaluation of three-dimensional sound intensity measurement accuracies and a proposal for an error correction method," Acoust. Sci. Tech. **34**, 34–41 (2013).
[23]C. P. Wiederhold, K. L. Gee, J. D. Blotter, and S. D. Sommerfeldt, "Comparison of methods for processing acoustic intensity from orthogonal multimicrophone probes," J. Acoust. Soc. Am. **131**, 2841–2852 (2012).
[24]K. Hori, "4 microphones power advanced, 3-dimensional sound intensity measuring system," J. Electron. Eng. **31**, 47–49 (1994).
[25]L. L. Locey, "Analysis and comparison of three acoustic energy density probes," M.S. thesis, Brigham Young University, Provo, UT (2004).
[26]G. Moschioni, B. Saggin, and M. Tarabini, "3-D sound intensity measurements: Accuracy enhancements with virtual-instrument-based technology," IEEE Trans. Instrum. Meas. **57**, 1820–1829 (2008).
[27]B. B. Monson, S. D. Sommerfeldt, and K. L. Gee, "Improving compactness for active noise control of a small axial cooling fan," Noise Control Eng. J. **55**, 397–407 (2007).
[28]T. W. Leishman, S. Rollins, and H. M. Smith, "An experimental evaluation of regular polyhedron loudspeakers as omnidirectional sources of sound," J. Acoust. Soc. Am. **120**, 1411–1422 (2006).
[29]P. M. Morse and K. U. Ingard, *Theoretical Acoustics* (McGraw-Hill, New York, 1968), pp. 418–421.
[30]G. W. Elko, "Biased against finite-difference bias," in *Proceedings of Noise-Con 91*, Tarrytown, NY (1991), pp. 541–546.
[31]H. Suzuki, S. Oguro, and T. Ono, "A sensitivity correction method for a three-dimensional sound intensity probe," J. Acoust. Soc. Jpn. **21**, 259–265 (2000).